

## Electronic Supplementary Information

### ***In situ* Protonation-Activated Supramolecular Self-assembly for Selective Suppression of Tumor Growth**

Xuan Wu<sup>a,c#</sup>, Ming Liu<sup>a#</sup>, Jie Niu<sup>b#</sup>, Qian Liu<sup>c</sup>, Xin Jiang<sup>d</sup>, Yujing Zheng<sup>a</sup>, Yuna Qian<sup>a,c</sup>, Ying-Ming Zhang<sup>b</sup>, Jianliang Shen<sup>\*a,c</sup>, Yu Liu<sup>\*b</sup>

<sup>a</sup> School of Ophthalmology & Optometry, School of Biomedical Engineering, Wenzhou Medical University, Wenzhou, Zhejiang 325035, China

E-mail: shenjl@wzucas.ac.cn (J. Shen)

<sup>b</sup> Department of Chemistry, State Key Laboratory of Elemento Organic Chemistry, Collaborative Innovation Center of Chemical Science and Engineering (Tianjin), Nankai University, Tianjin 300071, China

E-mail: yuliu@nankai.edu.cn (Y. Liu)

<sup>c</sup> University of the Chinese Academy of Sciences Wenzhou Institute, Wenzhou, Zhejiang 325000, China

<sup>d</sup> Department of Urology, Xiangya Hospital, Central South University, Changsha 410008, China.

#### Table of Contents

1. Materials and Methods.....	3
2. Synthesis and characterization of TPE-Py.....	4
3. <sup>1</sup> H NMR spectra of CB[8] and TPE-Py·HCl.....	5
4. Host-guest properties of CB[8] and TPE-Py·HCl.....	5
5. Fluorescence spectra of CB[8]⊃TPE-Py·HCl.....	7
6. Characterization of TPE-Py·HCl, CB[8]⊃TPE-Py·HCl assemblies.....	7
7. Zeta potential results of TPE-Py·HCl and CB[8]⊃TPE-Py·HCl.....	8
8. pH-responsive behavior of CB[8] and TPE-Py.....	8
10. Cell viability of TPE-Py and CB[8].....	10
11. Cell viability of TPE-Py·HCl and CB[8]⊃TPE-Py·HCl.....	11
12. Cellular uptake efficiency of TPE-Py.....	12
13. Confocal laser scanning images of RS1 cells.....	12
14. ROS generation ability of CB[8] and TPE-Py.....	12
15. Self-assembly behavior of TPE-Py and the mixture of TPE-Py and CB[8] at high concentration.....	13
16. Time-dependent images of A549 cells.....	13
17. Time-dependent bright-field images of CB[8] and TPE-Py.....	14
18. Lysosomal membrane permeabilization of A549 cells.....	14
19. Time-dependent images of lysosomes.....	14
20. <i>In vivo</i> toxicity tests.....	15
21. References.....	15

## 1. Materials and Methods

**Materials.** All reagents and solvents were used as received from commercial suppliers. All aqueous solutions were prepared with distilled water. A549 and RS1 cell lines were obtained from American Type Culture Collection (ATCC)

**Purification and characterization techniques.** Flash column chromatography was conducted with 200–300 mesh silica. UV–vis spectra were recorded in a quartz cell (light path = 1 cm) on a CARY5000 spectrophotometer. <sup>1</sup>H NMR spectra were recorded on a QUANTUM-I-400 MHz spectrometer. TEM pictures were obtained on an FEI Talos microscope at an accelerating voltage of 200 kV. Fluorescence emission spectra were measured on a FLUOROMAX-4 fluorescence spectrophotometer. SEM pictures were obtained with a JSM-7500F scanning electron microscope. Zeta potentials were measured with a Zeta PALS+BI-90 instrument (Brookhaven Co. USA).

**MTT assay.** The medium containing the cells at a density of  $8 \times 10^4$  was seeded in the 96-well plates, in which 100  $\mu$ L medium was placed per well, and the plates were cultured at 37 °C for 12 h at an atmosphere of 5% CO<sub>2</sub>. Then the serial solutions containing the test molecules, and the assembly were added to the plates, which were further incubated for a different time. After that, the culture medium was removed, followed by the addition of 100  $\mu$ L of MTT solution, which was incubated at 37 °C for another 4 h. Then the MTT formazan crystals were formed and dissolved by dimethyl sulfoxide (DMSO, 75  $\mu$ L). Finally, the OD value at 490 nm was recorded by a microplate reader (BioTek ELx808). The cells cultured in the fresh medium were set as the control group. The cytotoxicity was presented as the relative percentage of the cell viability compared with the control group.

**Colocalization experiment.** The A549 cells were seeded in plates at a density of  $2 \times 10^5$  cells per well in 0.5 mL of complete culture medium for 12 h before treatment. Then cells were treated with test molecules and the assembly. For A549 cells, the lysosomes were further labeled by LysoTracker DND-99 or the lysosome membrane dye (acridine orange) according to the provided instructions. Then, the cells were investigated by fluorescence microscopy (A1, Nikon, or STELLARIS 5, Leica).

**ROS generation.** The aqueous solution containing the tested systems was added. The 9,10-Anthracenediyl-bis(methylene)-dimalonic acid (ABDA), and irradiated under the high-pressure mercury lamp (300 W) at the visible light regions. Then the UV-vis spectra were recorded at intervals.

**Lysosomal membrane permeabilization.** Briefly, A549 cells plates at a density of  $2 \times 10^5$  cells per well in 0.5 mL of complete culture medium for 12 h before treatment. Then the cells were loaded with dextran fluorescein 10 KDa (FITC dextran) for 16 hours. Following a 6 hours chase period, a designated treatment was applied for 24 h. Then, the cells were investigated by fluorescence microscopy (A1, Nikon)

**Bio-TEM.** A549 cells were co-incubated with **TPE-Py** and **CB[8]** for 24h, respectively. The incubated cells were trypsinized and washed with PBS buffer before being fixed in glutaraldehyde (2.5%) overnight. The cells isolated from the fixing solution were washed by PBS buffer for 15 min (3 times) and further fixed by the solution of citric acid (1%) for 2h. Subsequently, the cells were washed with PBS buffer (3 times) and dehydrated with the mixtures of ethanol and PBS in a ratio gradient ranging from 30%, 50%, 70%, 80%, 90%, to 95% for 15 min in each case and neat ethanol and acetone for 20 min, respectively. The dehydrated cells were immersed in the EPON 812 resin washed with acetone. Sectioning the cells by a LEICA EM UC7 ultrathin slicer into 70-90 nm sections, which were further stained by the solution of lead citrate and the saturated solution of uranyl acetate in 50% ethanol for 10 min, respectively. Eventually, the bio-TEM images of the cells were recorded by FEI Talos microscope.

**XRD patterns.** The samples were prepared by freeze-drying, and the samples were analyzed at Bruker D8 ADVANCE. FT-IR spectra were recorded on Bruker Tensor II.

**Quantum chemical calculation.** All calculations are performed using Gaussian16 package. At the B3LYP/6-311G (d, p) level, the ground state structure is fully optimized using density functional theory (DFT), and the excited state energy levels are obtained using time-dependent density functional theory (TD-DFT). In order to consider the solvent effect, water is used as the solvent, all calculations are based on the polarizable continuum model (PCM).

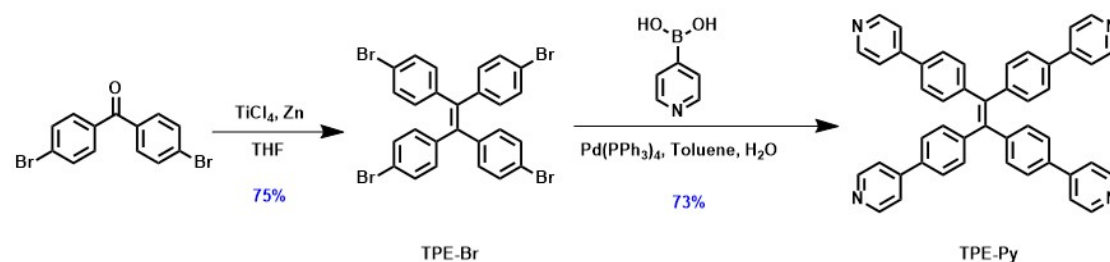
**Statistical analysis.** The results were expressed in the form of mean  $\pm$  standard deviation, in which at least three independent experiments were performed for the results. Tukey's test (Origin 8.0) was used for One-way analysis of variance. \*P < 0.05 was considered to be statistically significant.

**In vivo anti-tumor experiment.** To investigate the anti-tumor behavior *in vivo*, the A549 tumor model was established. Generally, nude mice were injected subcutaneously with  $5 \times 10^6$  A549 cells. Two weeks later, the mice bearing approximately 90 mm<sup>3</sup> tumors were randomly divided into four groups (n = 5). **TPE-Py** (75  $\mu$ M), **CB[8]** (300  $\mu$ M), and the mixture of **TPE-Py** (75  $\mu$ M) and **CB[8]** (300  $\mu$ M) were *in situ* administered 100  $\mu$ L every three days for 14 days and control mice were injected with the same volume of saline. During the treatment, no mice died in all groups. We measured the tumor volume and body weight of mice every two days, and the calculation of tumor volumes was according to the formula: Tumor volume (mm<sup>3</sup>) =  $0.5 \times (\text{Tumor width})^2 \times \text{Tumor length}$ . Finally, the mice were euthanized and the tumors were resected, taken photographs and weighed. The harvested tumor tissues and major organs (lung, heart spleen, liver, and kidney) were fixed using 4% para-formaldehyde for hematoxylin and eosin (H&E), Tunel, Ki67 staining. After being injected by **TPE-Py** and the mixture of **TPE-Py** and **CB[8]** for 24h. The tumors were collected and the *in vivo* imaging of tumors were performed on IVIS Lumina XRMS Series III, the fluorescence was collected at 600 nm, and the excitation

wavelength was 400 nm. The animal experiments were approved by the Animal Care and Use Committee at Wenzhou Institute, University of Chinese Academy of Sciences (Accreditation No. SYXK 2021-0040).

**In vivo safety evaluation.** To investigate the safety of **TPE-Py** and **CB[8]** *in vivo*, the mixture solution in PBS (100  $\mu$ L) of **TPE-Py** (75  $\mu$ M) and **CB[8]** (300  $\mu$ M) was injected into the Balb/C mice through the tail vein. The blood was collected after 2 h and 24 h respectively for the biochemical analysis, and major organs (lung, heart spleen, liver, and kidney) after 14 day for hematoxylin and eosin (H&E) staining. The animal experiments were approved by the Animal Care and Use Committee at Wenzhou Institute, University of Chinese Academy of Sciences (Accreditation No. SYXK 2021-0040).

## 2. Synthesis and characterization of TPE-Py



**Scheme S1.** Synthesis route of **TPE-Py**.

**TPE-Br**<sup>[S1]</sup>: Under the atmosphere of Ar, 4,4'-Dibromobenzophenone (3.50 g, 10.29 mmol) was dissolved in anhydrous THF (40 mL) and cool to -78 °C, followed by the addition of zinc powder (3.36 g, 25.73 mmol) and TiCl<sub>4</sub> (3.00 mL, 25.73 mmol). Then the mixture was refluxed for 12 h and cooled to 25 °C, which was quenched by 1N HCl, after the removal of THF under reduced pressure, the mixture was extracted by dichloromethane (50 mL  $\times$  3). The organic phase was combined and washed by water and saturated brine, respectively, and dried over anhydrous MgSO<sub>4</sub>. The **TPE-Br** was obtained by column chromatography (petroleum ether) as the white solid (2.53 g, 7.6 mmol, 75% yield). <sup>1</sup>H NMR (400 MHz, CDCl<sub>3</sub>, 298 K)  $\delta$  (ppm) = 7.30 (d, *J* = 8.5 Hz, 8H), 6.88 (d, *J* = 8.5 Hz, 8H).

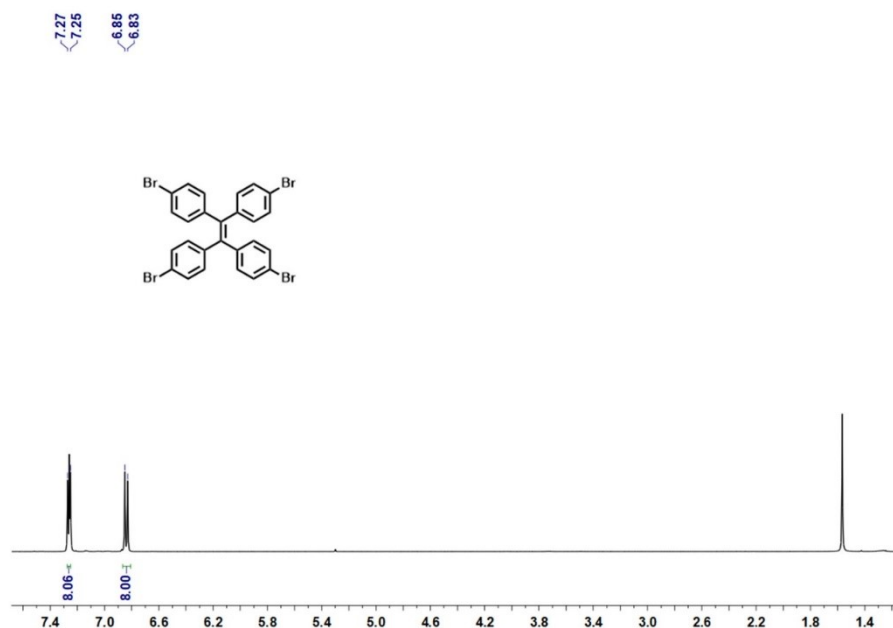


**Figure S1.** <sup>1</sup>H NMR spectrum (400 MHz, CDCl<sub>3</sub>, 298 K) of **TPE-Br**.

**TPE-Py**<sup>[S2]</sup>: Under the atmosphere of Ar, tetrakis(4-bromophenyl)ethene (1.00 g, 1.54 mmol), 4-pyridinylboronic acid (1.14 g, 9.26 mmol), K<sub>2</sub>CO<sub>3</sub> (2.56 g, 18.52 mmol), Pd(PPh<sub>3</sub>)<sub>4</sub> (356.64 mg, 0.308 mmol) were added into a 250 mL three necked flask. Then toluene (60 mL), and water (60 mL) were added and the reaction was refluxed at 120 °C for 3 days. After cooling to 25 °C, the solvents were removed and the residue was purified by flash column chromatography (CH<sub>2</sub>Cl<sub>2</sub>:MeOH = 10:1) to give compound **TPE-Py** as a faint yellow solid (0.726 g, 1.12 mmol, 73% yield). <sup>1</sup>H NMR (400 MHz, CDCl<sub>3</sub>, 298 K)  $\delta$  (ppm) = 8.66 (d, *J* = 4.8 Hz, 8H), 7.55 – 7.49 (m, 16H), 7.26 (d, *J* = 8.2 Hz, 8H).

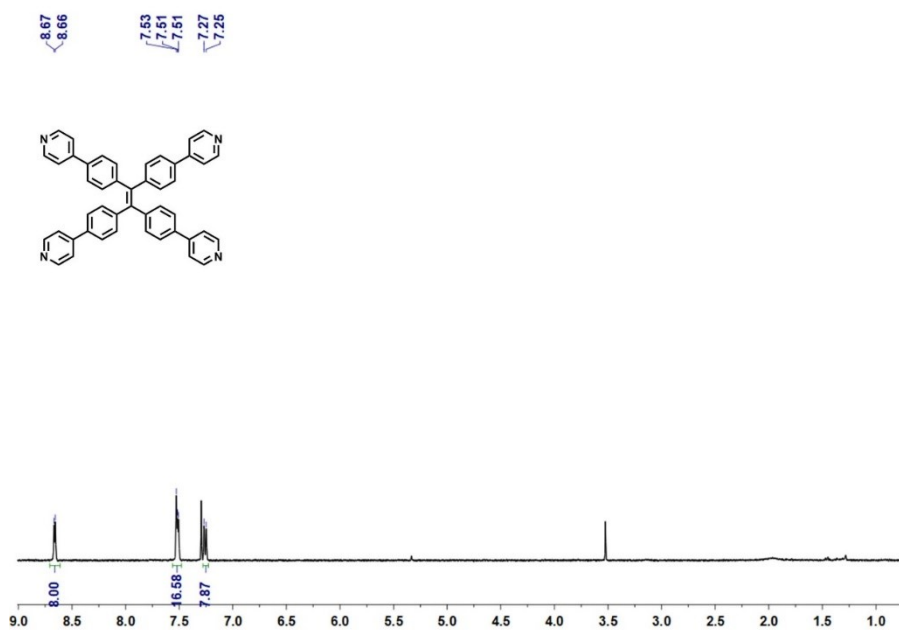


Figure S2.  $^1\text{H}$  NMR spectrum (400 MHz,  $\text{CDCl}_3$ , 298 K) of TPE-Py.

### 3. $^1\text{H}$ NMR spectra of CB[8] and TPE-Py·HCl

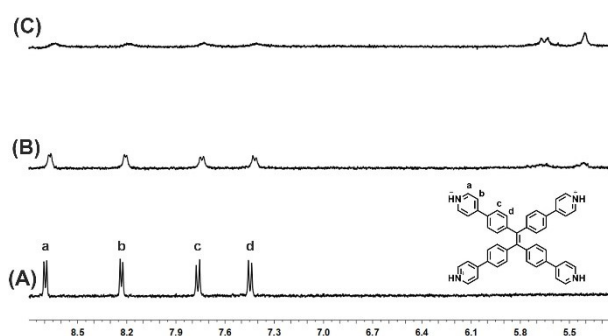


Figure S3. Partial  $^1\text{H}$  NMR (400 MHz, 298 K,  $\text{D}_2\text{O}$ ) spectrum of (A) TPE-Py·HCl, (B) TPE-Py·HCl]:[CB[8]] = 1:0.5, and (C) [TPE-Py·HCl]:[CB[8]] = 1:1 ([TPE-Py·HCl] = 0.4 mM, pD = 1.0).

### 4. Host-guest properties of CB[8] and TPE-Py·HCl

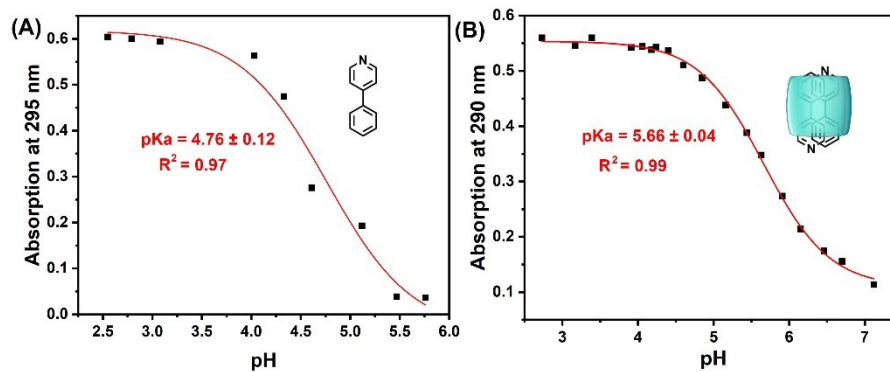
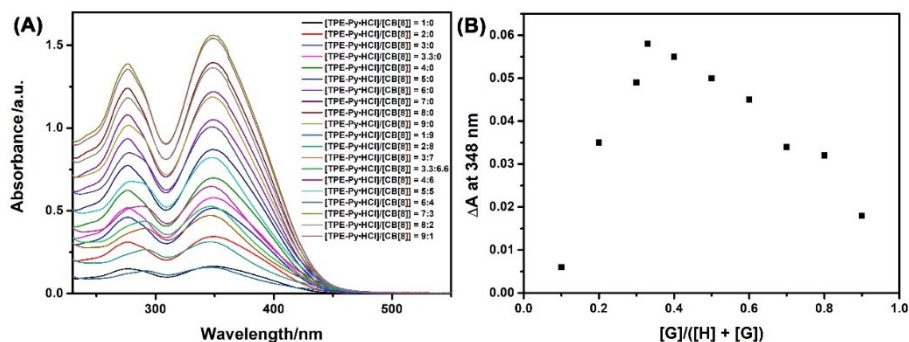
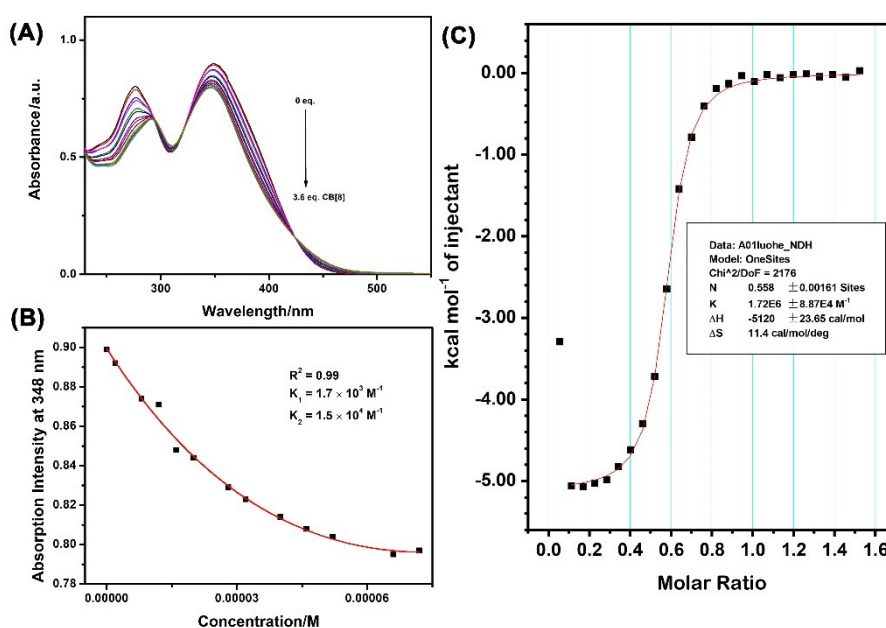


Figure S4.  $\text{pK}_a$  values of (a) MG, (B) MG in presence of CB[8] ([MG] = 0.04 mM, [CB[8]] = 0.02 mM).



**Figure S5.** (A) UV-Vis spectra of the **CB[8]** and **TPE-Py·HCl** in water (pH = 3.0) at different molar ratios while  $[\text{CB[8]}] + [\text{TPE-Py·HCl}] = 4 \times 10^{-5} \text{ M}$ . (b) Job's Plot showing 2:1 stoichiometry of the complex between **CB[8]** and **TPE-Py·HCl** by plotting the difference adsorption intensity at 348 nm against the molar fraction of **G** at an invariant total concentration of  $4 \times 10^{-5} \text{ M}$  in aqueous solution (pH = 3.0).



**Figure S6.** (A) UV-Vis spectra of **TPE-Py·HCl** at a concentration of  $2 \times 10^{-5} \text{ M}$  in aqueous solution (pH = 3.0) upon the gradual addition of **CB[8]** from 1 to 3.6 eq., (B) the adsorption change of **TPE-Py·HCl** at 348 nm upon the addition of **CB[8]** ( $0-7.2 \times 10^{-5} \text{ M}$ , pH = 3.0), (C) ITC data for the titration of **CB[8]** (0.1 mM) in the cell with a solution of **TPE-Py·HCl** (0.8 mM) in the syringe in  $\text{H}_2\text{O}$  at  $25 \text{ }^\circ\text{C}$  (pH = 1.0). The red solid curve was obtained from the nonlinear curve-fitting.

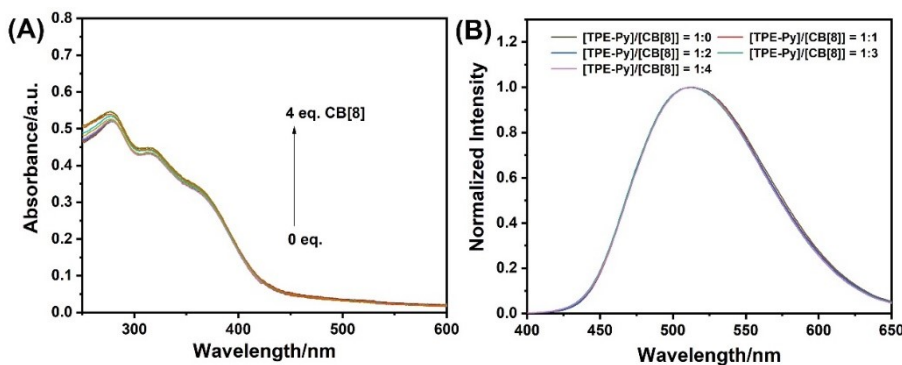


**Figure S7.** (A) UV-Vis spectra of **TPE-Py** at a concentration of  $2 \times 10^{-5} \text{ M}$  in aqueous solution (pH = 7.4) upon the gradual addition of **CB[8]** from 1 to 4.0 eq., (B) Normalized fluorescence spectra of **TPE-Py** at a concentration of  $2 \times 10^{-5} \text{ M}$  in aqueous solution upon the gradual addition of **CB[8]** from 0 to 4.0 eq (pH = 7.4).

## 5. Fluorescence spectra of CB[8]⊃TPE-Py·HCl

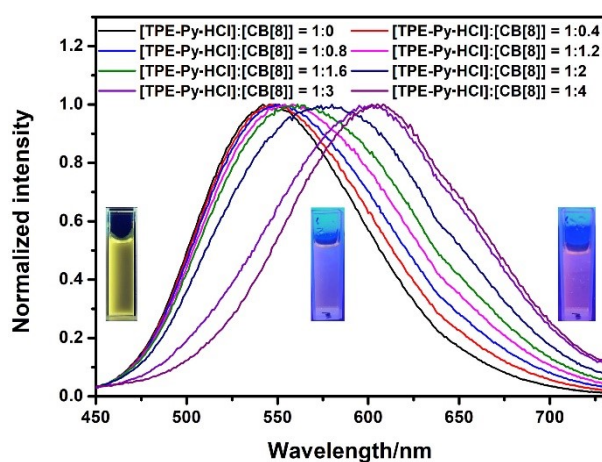


Figure S8. Normalized fluorescence spectra of TPE-Py·HCl at a concentration of  $2 \times 10^{-5}$  M in aqueous solution upon the gradual addition of CB[8] from 0 to 4.0 eq (pH = 3.0).

## 6. Characterization of TPE-Py·HCl, CB[8]⊃TPE-Py·HCl assemblies

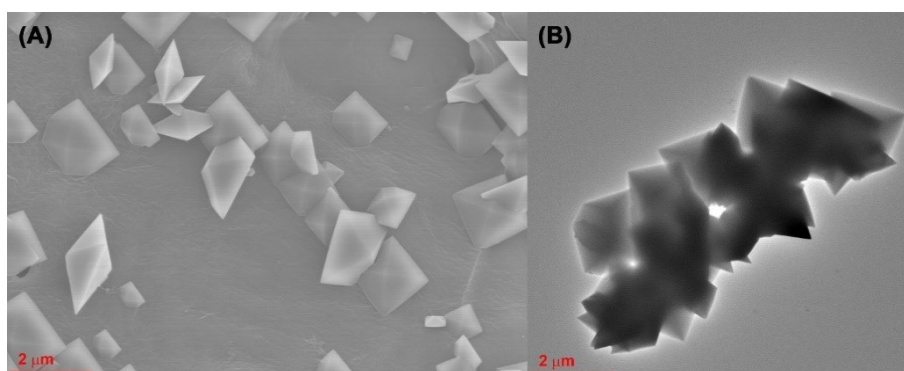


Figure S9. SEM image (A) and TEM image (B) of CB[8] and TPE-Py·HCl ([TPE-Py·HCl]:[CB[8]] = 1:4).

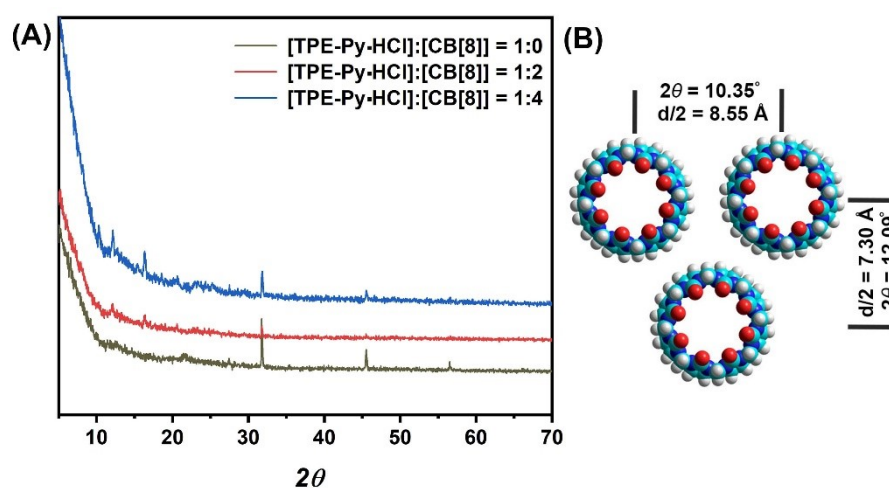


Figure S10. Powder XRD profiles of nanostructures in the solid states. (B) Possible stacking manners between host-guest complex concluded from XRD results..

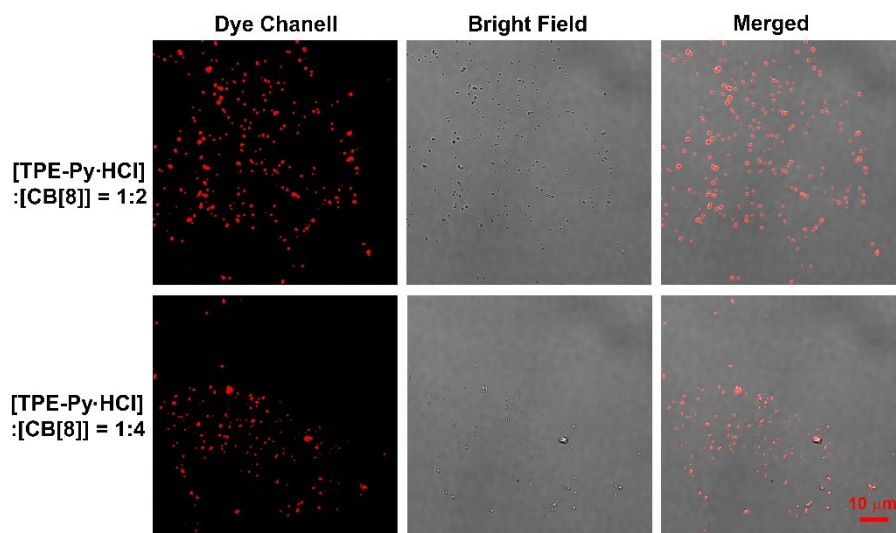


Figure S11. Confocal laser scanning images of CB[8]@TPE-Py·HCl at different molar ratios.

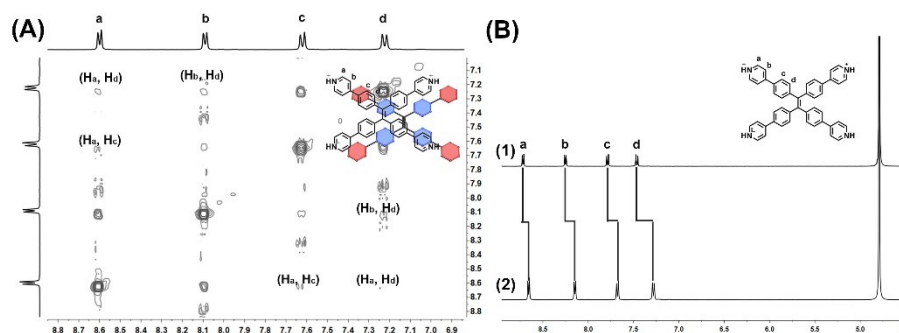


Figure S12. (A) 2D NOESY (400 MHz, D<sub>2</sub>O, 298 K, pD = 2.5) spectrum of TPE-Py·HCl, (B) <sup>1</sup>H NMR (400 MHz, D<sub>2</sub>O, 298 K) spectra of TPE-Py·HCl at different concentration (1) 0.5 mM, pD = 2.5, (2) 4 mM, pD = 2.5.

## 7. Zeta potential results of TPE-Py·HCl and CB[8]@TPE-Py·HCl

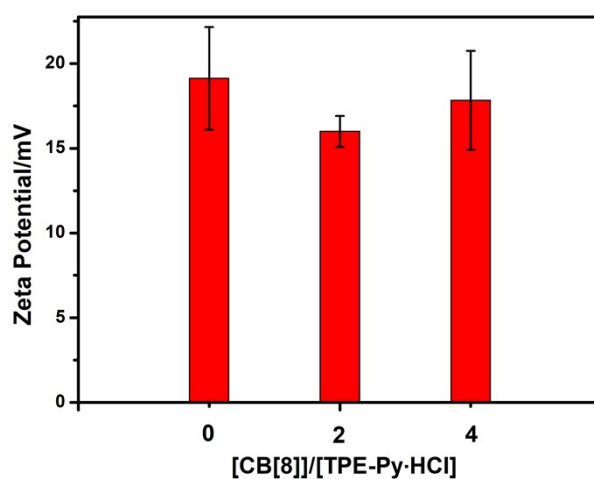
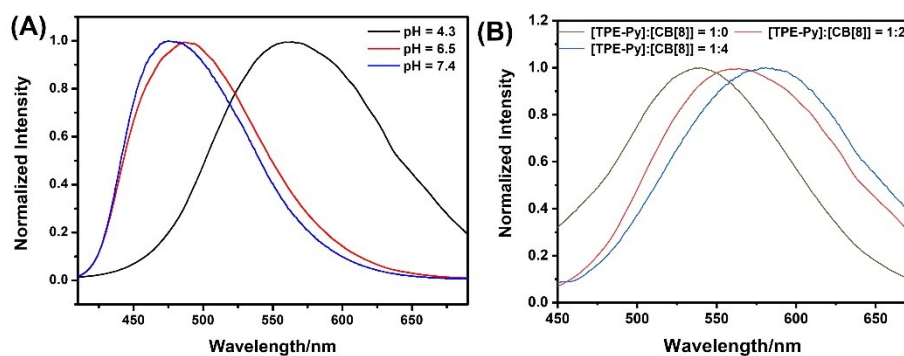
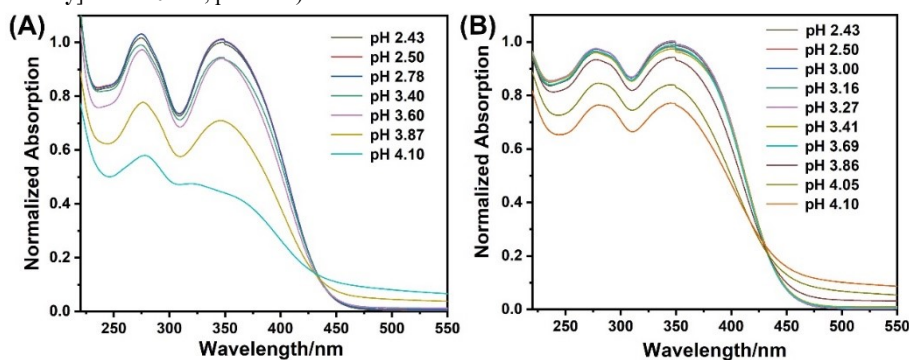


Figure S13. Zeta potential of TPE-Py·HCl and CB[8]@TPE-Py·HCl. (Data were presented as mean  $\pm$  SD ( $n = 3$ )).

## 8. pH-responsive behavior of CB[8] and TPE-Py



**Figure S14.** (A) Normalized fluorescence spectra of TPE-Py and CB[8] in the aqueous solution with different pH value ( $[TPE-Py] = 2 \times 10^{-5} M$ ,  $[CB[8]] = 4 \times 10^{-5} M$ ), (B) Normalized fluorescence spectra of TPE-Py and CB[8] in the aqueous solution ( $[TPE-Py] = 2 \times 10^{-5} M$ , pH = 4.2)



**Figure S15.** Normalized UV-Vis spectra of (A) TPE-Py·HCl, (B) CB[8]⊃TPE-Py·HCl in different pH solution ( $[TPE-Py \cdot HCl] = 0.02 \text{ mM}$ ,  $[CB[8]] = 0.04 \text{ mM}$ ).

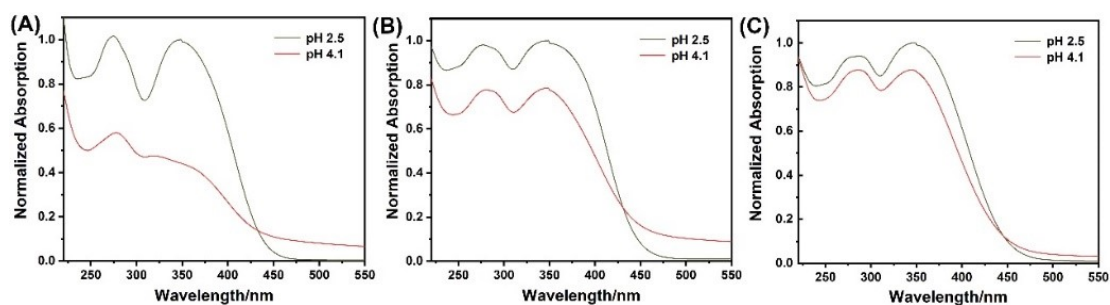


**Figure S16.** Normalized UV-Vis spectra of (A) TPE-Py·HCl, (B) CB[8]⊃TPE-Py·HCl ( $[CB[8]]:[TPE-Py \cdot HCl] = 2:1$ ), (C) CB[8]⊃TPE-Py·HCl ( $[CB[8]]:[TPE-Py \cdot HCl] = 4:1$ ) in different pH solution ( $[TPE-Py \cdot HCl] = 0.02 \text{ mM}$ )

## 9. pH-Responsive ROS generation ability of TPE-Py and CB[8]

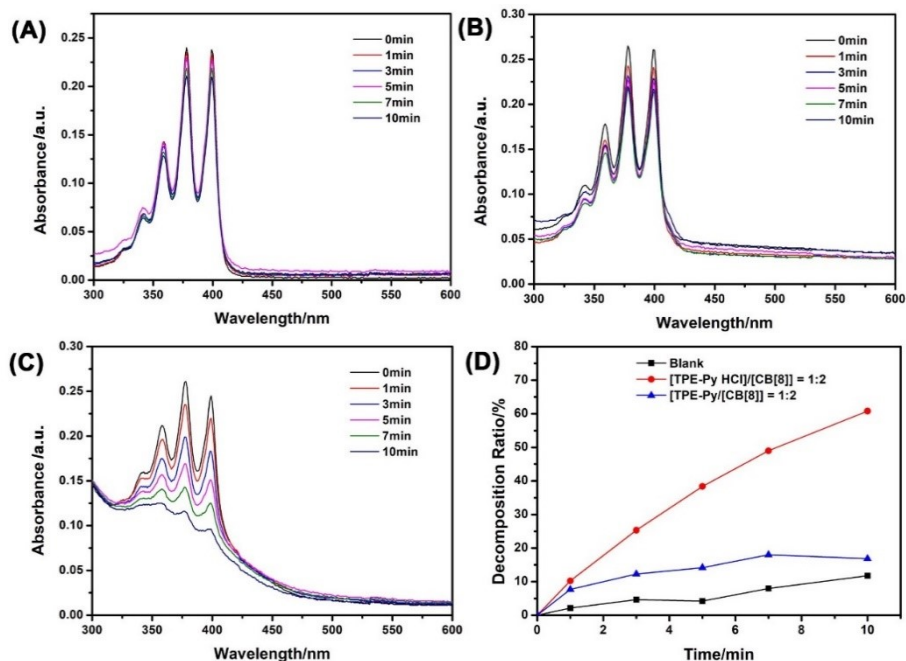


**Figure S17.** Time-dependant UV-Vis spectra of ABDA under the irradiation of white light, (A) ABDA solution, (B) ABDA solution with TPE-Py and CB[8], and (C) ABDA solution with TPE-Py·HCl and CB[8], and (D) decomposition ratio of ABDA calculated by the absorption change at 375 nm. ( $[ABDA] = 2 \times 10^{-5}$  M,  $[TPE-Py] = 2 \times 10^{-6}$  M,  $[TPE-Py \cdot HCl] = 2 \times 10^{-6}$  M, and  $[CB[8]] = 4 \times 10^{-6}$  M.)

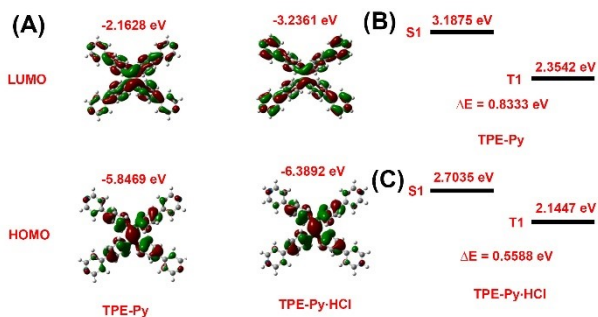


**Figure S18.** (A) The calculated HOMO and LUMO orbits of TPE-Py and TPE-Py·HCl, (B) the S1 and T1 energy gap of TPE-Py, (C) the S1 and T1 energy gap of TPE-Py·HCl (Gaussian 16, B3LYP/6-311G (d, p)).

## 10. Cell viability of TPE-Py and CB[8]

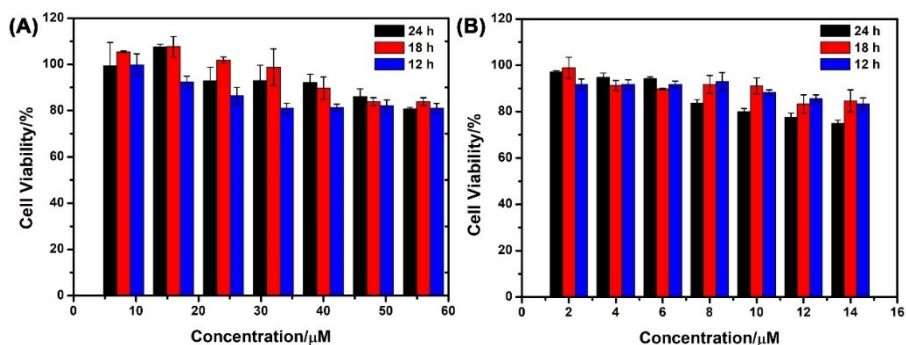


**Figure S19.** Concentration-dependent cell viability of A549 cancer cells incubated with (A) CB[8], (B) TPE-Py for different time points under the indicated concentrations. (Data were presented as mean  $\pm$  SD ( $n = 3$ )).

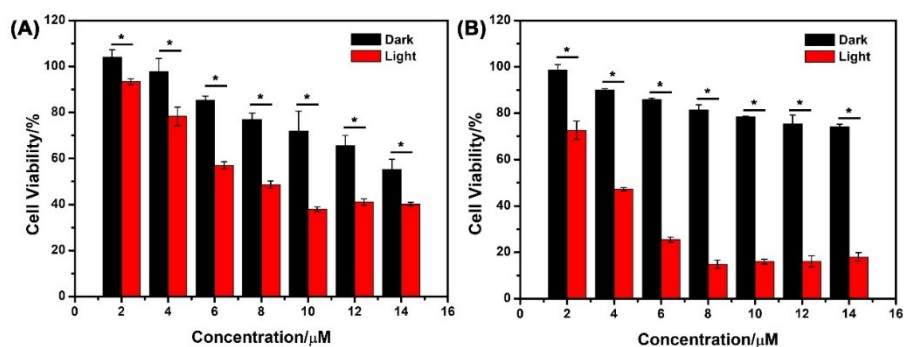


**Figure S20.** (A) Concentration-dependent relative cell viability of A549 cancer cells incubated with TPE-Py and CB[8] at the molar ratio of 1:4 for 18 h (the white light irradiation time was 10 min,  $*P < 0.05$ .), and (B) concentration-dependent relative cell viability of A549 cancer cells incubated with TPE-Py and CB[8] at the molar ratio of 1:4 for 12 h (the white light irradiation time was 10 min. Data were presented as mean  $\pm$  SD ( $n = 3$ ),  $*P < 0.05$ ).

### 11. Cell viability of TPE-Py·HCl and CB[8] $\supset$ TPE-Py·HCl

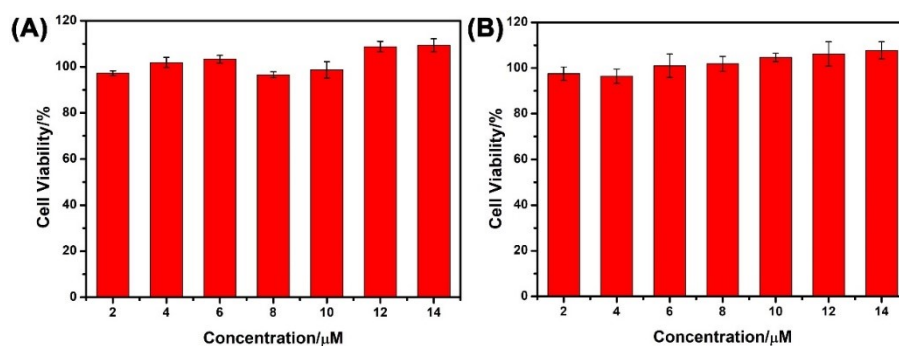


**Figure S21.** Concentration-dependent cell viability of A549 cancer cells incubated with (A) TPE-Py·HCl, and (B) CB[8] $\supset$ TPE-Py·HCl at the molar ratio of 1:4 for 24 h. (The concentration was determined by TPE-Py·HCl. Data were presented as mean  $\pm$  SD ( $n = 3$ ).

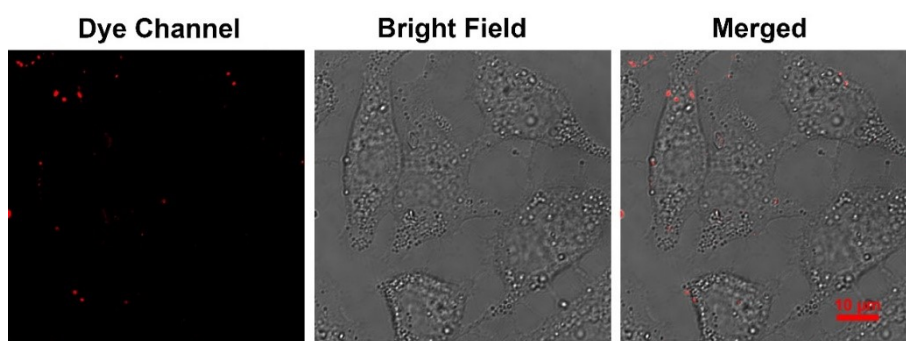


**Figure S22.** Confocal laser scanning images of A549 cancer cells after being incubated with CB[8] $\supset$ TPE-Py·HCl for 24h. ([TPE-Py·HCl] = 6  $\mu\text{M}$ , [CB[8]] = 24  $\mu\text{M}$ )

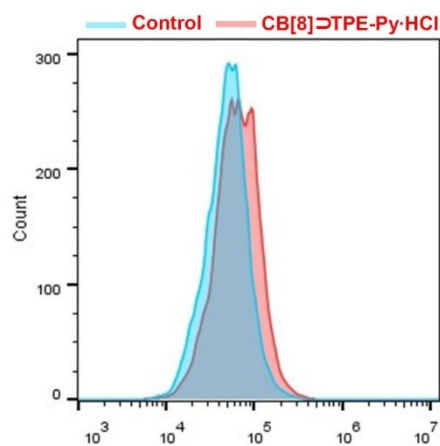


**Figure S23.** Fluorescence intensity of A549 cells was analyzed by flow cytometry at different time points after being incubated with  $\text{CB}[8]\supset\text{TPE-Py-HCl}$  ( $[\text{CB}8] = 24 \mu\text{M}$ ,  $[\text{TPE-Py-HCl}] = 6 \mu\text{M}$ , the fluorescence was collected in the channel of Violet 610).

## 12. Cellular uptake efficiency of TPE-Py

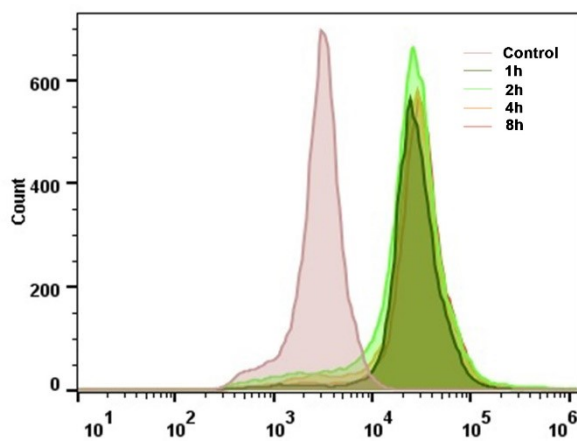


**Figure S24.** Fluorescence intensity of A549 cells was analyzed by flow cytometry at different time points after being incubated with  $\text{TPE-Py}$  ( $[\text{TPE-Py}] = 4 \mu\text{M}$ , the fluorescence was collected in the channel of PB450).

## 13. Confocal laser scanning images of RS1 cells

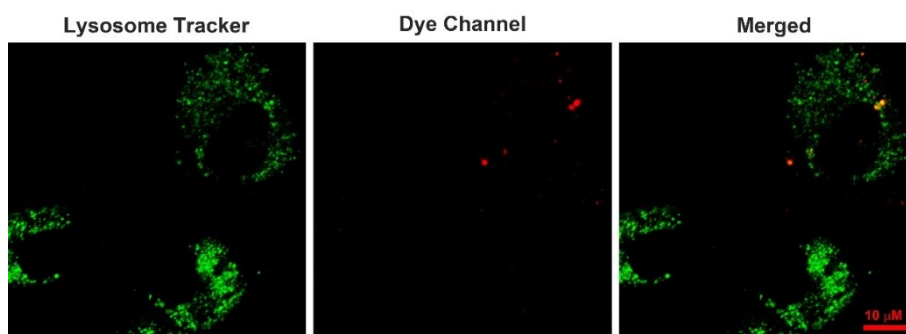


**Figure S25.** Confocal laser scanning images of RS1 cells after being incubated with  $\text{CB}[8]\supset\text{TPE-Py}$  for 24h. ( $[\text{TPE-Py}] = 6 \mu\text{M}$ ,  $[\text{CB}[8]] = 24 \mu\text{M}$ )

## 14. ROS generation ability of $\text{CB}[8]$ and $\text{TPE-Py}$

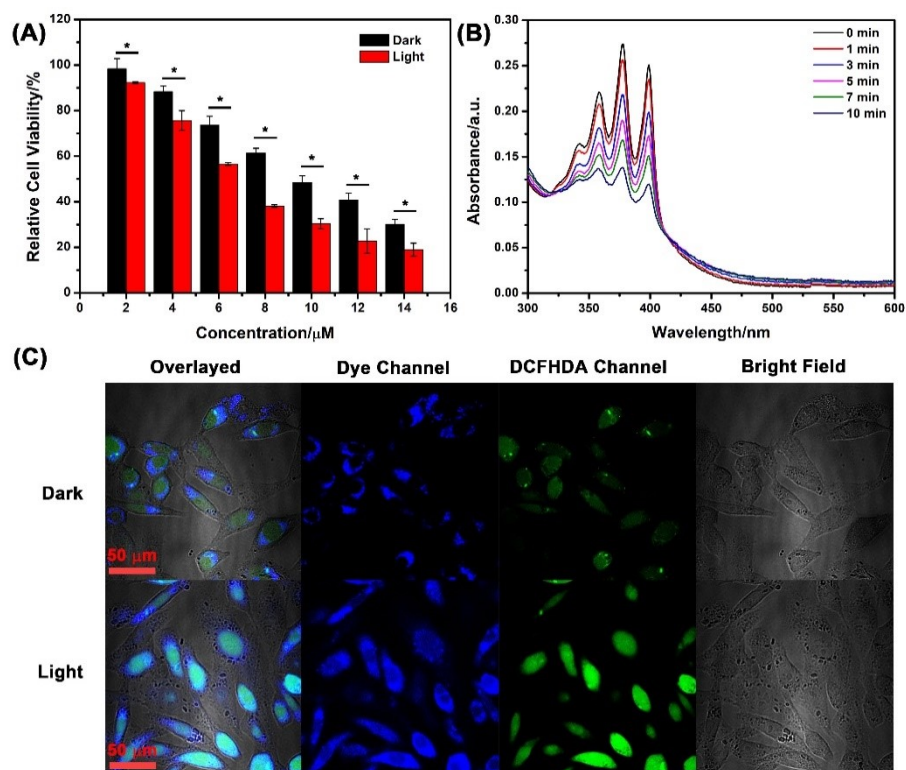


**Figure S26.** (A) Concentration-dependent relative cell viability of A549 cancer cells with or without the irradiation of white light for 10 min ( $[\text{CB}8]/[\text{TPE-Py}] = 4:1$ , and the concentration was settled by the concentration of **TPE-Py**, the incubation time was 24 h), (B) Time-dependent UV-Vis spectra of ABDA under the irradiation of white light in the presence of  $\text{CB}[8] \supset \text{TPE-Py} \cdot \text{HCl}$  ( $[\text{ABDA}] = 2 \times 10^{-5} \text{ M}$ ,  $[\text{TPE-Py}] = 2 \times 10^{-6} \text{ M}$ ,  $[\text{TPE-Py} \cdot \text{HCl}] = 2 \times 10^{-6} \text{ M}$ , and  $[\text{CB}[8]] = 8 \times 10^{-6} \text{ M}$ ), and (C) Confocal laser scanning images of DCFH-DA on A549 cancer cells. (Data were presented as mean  $\pm$  SD ( $n = 3$ ), \* $P < 0.05$ )

### 15. Self-assembly behavior of TPE-Py and the mixture of TPE-Py and CB[8] at high concentration.

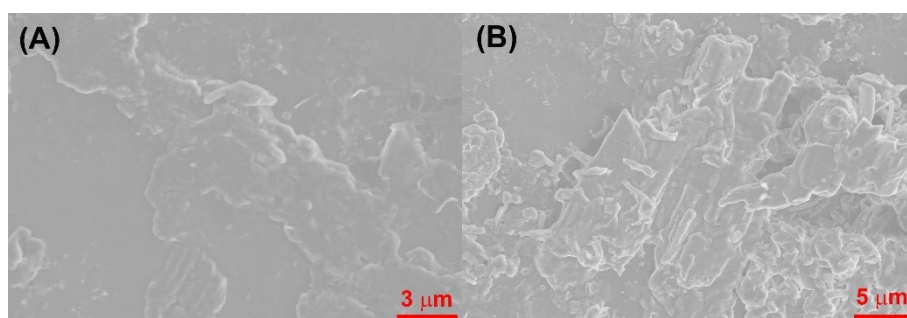


**Figure S27.** SEM images of (A) TPE-Py, and (B) TPE-Py and CB[8] in the concentrated solution ( $[\text{TPE-Py}] = 20 \mu\text{M}$ ,  $[\text{CB}[8]] = 80 \mu\text{M}$ )

### 16. Time-dependent images of A549 cells

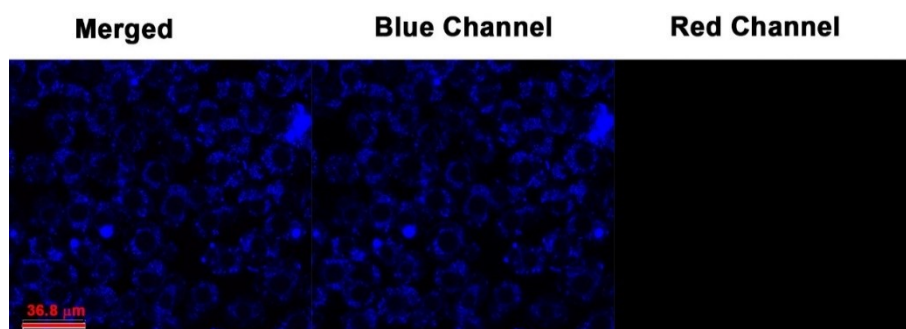


**Figure S28.** Confocal laser scanning images of A549 cancer cells incubated with TPE-Py for 24 h ( $[TPE-Py] = 8 \mu M$ ). The signal of the blue channel was collected from 425 nm to 525 nm, and the red channel was collected from 551 nm to 650 nm.

### 17. Time-dependent bright-field images of CB[8] and TPE-Py

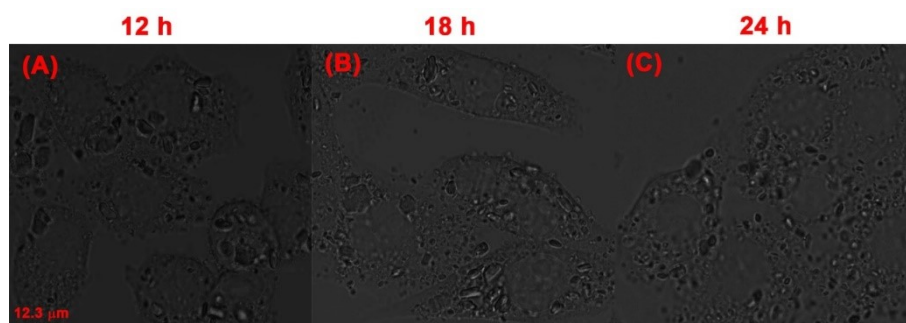


**Figure S29.** The bright-field image of A549 cancer cells was incubated with CB[8] and TPE-Py at different time points. ( $[TPE-Py] = 8 \mu M$ ,  $[CB[8]] = 32 \mu M$ )

### 18. Lysosomal membrane permeabilization of A549 cells

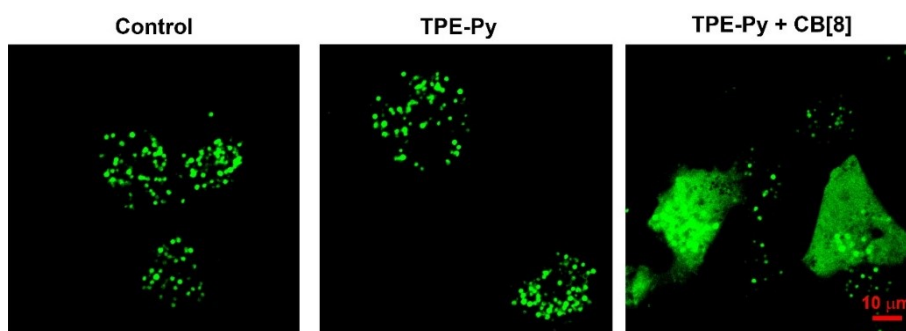


**Figure S30.** Fluorescence images of A549 cells loading with FITC-dextran (10 KDa) for 16 hour, and treated with TPE-Py and the mixture of TPE-Py and CB[8] for 24h. ( $[TPE-Py] = 10 \mu M$ ,  $[CB[8]] = 40 \mu M$ )

### 19. Time-dependent images of lysosomes

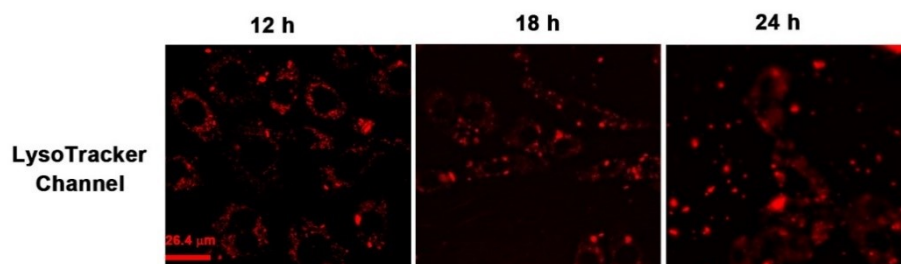


**Figure S31.** Confocal laser scanning images of lysosomes changes of A549 cancer cells ([TPE-Py] = 12  $\mu$ M, [CB[8]] = 48  $\mu$ M).

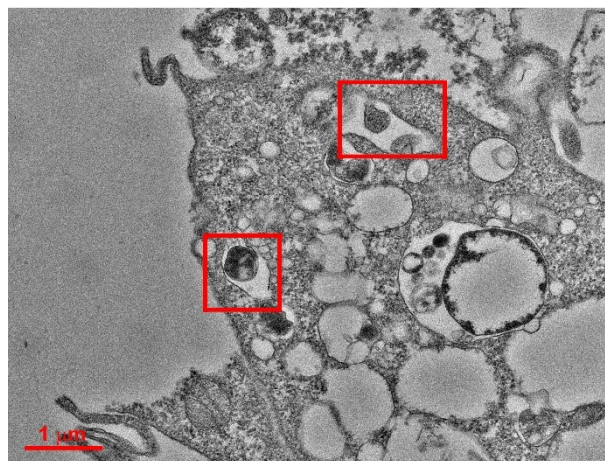


**Figure S32.** Bio-TEM images of impaired lysosomes.

## 20. *In vivo* toxicity tests

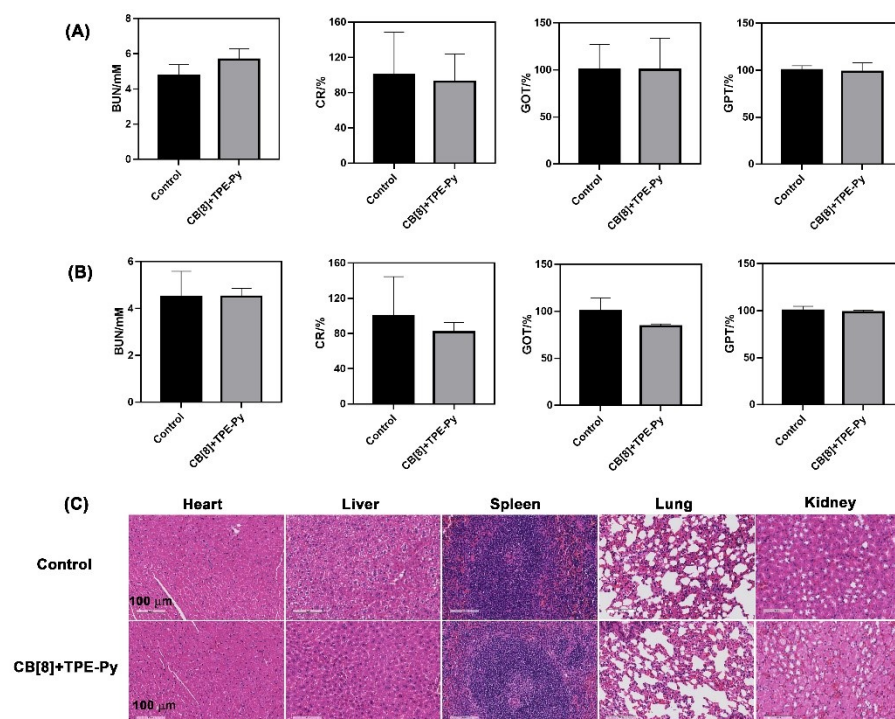


**Figure S33.** Serum biochemistry data of GOT, GPT, BUN and CR reflecting reflecting liver function and kidney function (n = 3) (A) data collected at (A) 2 h and (B) 24 h after the tail vein injection, (C) H&E staining images of Liver, Heart, Spleen, Kidney, and Lung on Day 14.

## 21. References

- [S1] B. C. Patra, S. Bhattacharya, *Chem. Mater.* 2021, **33**, 8512.
- [S2] S.-S. Zhao, L. Chen, L. Wang, Z. Xie, *Chem. Commun.* 2017, **53**, 7048.